Two-dimensional polymer grating and prism on Bloch surface waves platform

Libo Yu, Elsie Barakat,* Joab Di Francesco, and Hans Peter Herzig

Ecole Polytechnique Fédérale de Lausanne, Optics and Photonics Technology Laboratory, Maladière 71, 2000 Neuchâtel, Switzerland

*elsie.barakat@epfl.ch

Abstract: A one-dimensional photonic crystal sustaining Bloch Surface Waves (BSWs) is used as a platform for two-dimensional integrated optics. The dielectric platform shows low loss, long propagation distance and high surface field enhancement. In order to study the potential of the platform for future photonic chips, polymer ultra-thin prisms and gratings (~ 100 *nm*) are engineered on the top of the platform. This polymer layer modifies the BSWs effective index enabling a direct manipulation of light. The BSW deflection effects caused by surface prisms are observed in the near-field and Snells law is verified; then the BSW diffractions through surface gratings are experimentally and theoretically characterized. The results show a robust platform that can be used for integrated optics that includes different optical components. One of the main advantages is that these 2*D* photonic devices can have arbitrary shapes, which is difficult to obtain in 3*D*.

OCIS codes: (140.3490) Lasers, distributed-feedback; (240.6690) Surface waves; (050.0050) Diffraction and gratings; (130.0130) Integrated optics; (220.0220) Optical design and fabrication.

References and links

1. W. Knoll, "Interfaces and thin films as seen by bound electromagnetic waves," Ann. Rev. Phys. Chem. **49**, 569–638 (1998).
2. A. Zayats and I. Smolyaninov, "Near-field photonics: surface plasmon polaritons and localized surface plasmons," J. Opt. A.: Pure Appl. Opt. **5**, S16–S50 (2003).
3. W. L. Barnes, A. Dereux, and T. W. Ebbesen, "Surface plasmon subwavelength optics," Nature **424**, 824–830 (2003).
4. L. Yu, E. Barakat, T. Sfez, L. Hvozdara, J. Di Francesco, and H.-P. Herzig, "Manipulating Bloch surface waves in 2*D* a platform concept based flat lens and resonators," Light: Sci. Appl. **124**, e124 (2014).
5. F. Giorgis, E. Descrovi, C. Summonte, L. Dominici, and F. Michelotti, "Experimental determination of the sensitivity of Bloch surface waves based sensors," Opt. Express **20**, 8087–8093(2010).
6. L. Yu, T. Sfez, V. Paeder, P. Stenberg, W. Nakagawa, M. Kuittinen, and H. P. Herzig, "Direct comparison of the performance of Bloch surface wave and surface plasmon polariton sensors," Sens. Actuat. B: Chem. **174**, 292–298 (2012).
7. N. Danz, A. Sinibaldi, F. Michelotti, E. Descrovi, P. Munzert, P. Munzert, and U. Sculz, "Improving the sensitivity of optical biosensors by means of Bloch surface waves," Biomed. Tech. **57**, 584–587 (2012).
8. M. Liscidini and J. E. Sipe, "Analysis of Bloch-surface-wave assisted diffraction-based biosensors," J. Opt. Soc. Am. B. **2**, 279–289 (2009).
9. V. Paeder, V. Musi, L. Hvozdara, S. Herminjard, and H. P. Herzig, "Detection of protein aggregation with a Bloch surface wave based sensor," Sen. Actuat. B: Chem. **157**, 260–264 (2011).
10. V. N. Konopsky, T. Karakouz, E. V. Alieva , C. Vicario, S. K. Sekatskii, and G. Dietler, "Photonic crystal biosensor based on optical surface waves," Sensors **13**, 2566–2578 (2013).

#250804 Received 25 Sep 2015; revised 18 Nov 2015; accepted 19 Nov 2015; published 30 Nov 2015

11. L. Yu, T. Sfez, V. Paeder, P. Stenberg, W. Nakagawa, M. Kuittinen, and H. P. Herzig, "Fast optical vapour sensing by Bloch surface waves on porous silicon membranes," Phys. Chem. Chem. Phys. **12**, 502–506 (2010).
12. I. V. Soboleva, E. Descrovi, C. Summonte, A. A. Fedyanin, and F. Giorgis, "Fluorescence emission enhanced by surface electromagnetic waves on one-dimensional photonic crystals," Appl. Phys. Lett. **94**, 231122 (2009).
13. M. Ballarini, F. Frascella, N. De Leo, S. Ricciardi, P. Rivolo, P. Mandracci, E. Enrico, F. Giorgis, F. Michelotti, and E. Descrovi, "A polymer-based functional pattern on one-dimensional photonic crystals for photon sorting of fluorescence radiation," Opt. Express **20**, 6703–6711 (2012).
14. E. Descrovi, T. Sfez, M. Quaglio, D. Brunazzo, L. Dominici, F. Michelotti, H.-P. Herzig, O. Martin, and F. Giorgis, "Guided Bloch surface waves on ultrathin polymeric ridges," Nano Lett. **10**, 2087–2091 (2010).
15. T. Sfez, E. Descrovi, L. Yu, D. Brunazzo, M. Quaglio, L. Dominici, W. Nakagawa, F. Michelotti, F. Giorgis, O. J. F. Martin, and H.-P. Herzig, "Bloch surface waves in ultrathin waveguides: near-field investigation of mode polarization and propagation," J. Opt. Soc. Am. B **27**, 1617–1625 (2010).
16. M. Menotti and M. Liscidini, "Optical resonators based on Bloch surface waves," J. Opt. Soc. Am. B **32**, 431 (2015).
17. L. Yu, T. Sfez, V. Paeder, P. Stenberg, W. Nakagawa, M. Kuittinen, and H. P. Herzig, "Concurrent polarization retrieval in multi-heterodyne scanning near-field optical microscopy: validation on silicon form-birefringent grating," Opt. Express **20**, 23088–23099 (2012).
18. M. Ballarini, F. Frascella, E. Enrico, P. Mandracci, N. De Leo, F. Michelotti, F. Giorgis, and E. Descrovi, "Bloch surface waves-controlled fluorescence emission: coupling into nanometer-sized polymeric waveguides," Appl. Phys. Lett. **100**, 063305 (2012).
19. H. Wei and H. Xu, "Controlling surface plasmon interference in branched silver nanowire structures," Nanoscale **4**, 7149–7154 (2012).
20. X. Li, Q. Tan, B. Bai, and G. Jin, "Experimental demonstration of tunable directional excitation of surface plasmon polaritons with a subwavelength metallic double slit," Appl. Phys. Lett. **98**, 251109 (2011).
21. Z. Liu, J. M. Steele, W. Srituravanich, Y. Pikus, C. Sun, and X. Zhang, "Focusing surface plasmons with a plasmonic lens," Nano Lett. **5**, 1726–1729 (2005).
22. Y. Li, T. Yang, Z. Pang, G. Du, S. Song, and S. Han, "Phase-sensitive Bloch surface wave sensor based on variable angle spectroscopic ellipsometry," Opt. Express **22**, 21403–21410 (2014).
23. J. Lin, J. Dellinger, P. Genevet, B. Cluzel, F. de Fornel, and F. Capasso, "Cosine-Gauss plasmon beam: a localized long-range nondiffracting surface wave," Phys. Rev. Lett. **109**, 093904 (2012).
24. Z. Fang, Q. Peng, W. Song, F. Hao, J. Wang, P. Nordlander, and X. Zhu, "Plasmonic focusing in symmetry broken nanocorrals," Nano Lett. **11**, 893–897 (2011).
25. E. Devaux, J.-Y. Laluet, B. Stein, C. Genet, T. Ebbesen, J.-C. Weeber, and A. Dereux, "Refractive micro-optical elements for surface plasmons: from classical to gradient index optics," Opt. Express **18**, 20610–20619 (2010).
26. L. Yin, V. K. Vlasko-Vlasov, J. Pearson, J. M. Hiller, J. Hua, U. Welp, D. E. Brown, and C. W. Kimball, "Subwavelength focusing and guiding of surface plasmons," Nano Lett. **5**, 1399–1402 (2012).
27. S. I. Bozhevolnyi, V. S. Volkov, E. Devaux, J.-Y. Laluet, and T. W. Ebbesen, "Channel plasmon subwavelength waveguide components including interferometers and ring resonators," Nature **440**, 508–511 (2006).

1. Introduction

Nano-photonics, where optical nano-materials can slow down, trap and manipulate light at the sub-wavelength scale, has become a major research area and is making important advances towards optical communications, nano-imaging and sensing. In particular, two-dimensional (2*D*) concepts are interesting to realize fully integrated systems and to align components at the nanoscale. The third dimension can be used for monitoring light propagation or for sensing applications. There are few ways of addressing a 2*D* optical environment. One of the methods is represented by the well-known Surface Plasmon Polaritons (SPPs) on planar or structured metallic surfaces. SPPs are electromagnetic modes sustained at a metallic/dielectric interface resulting in low quality factor [1–3]. However, the propagation length of SPPs is limited by high absorption losses in metals. A novel low-cost platform suitable for fundamental investigations of light propagation through micro- and nano-structures has been recently proposed [4]. The presented 2*D* concept based on Bloch Surface Waves (BSWs) is a strong candidate to realize fundamental experiments, as well as entire photonic systems. This platform is based on a dielectric multilayer that sustains Bloch surface waves (BSWs). BSWs are electromagnetic surface waves excited at the interface between a truncated periodic dielectric multilayer and a surrounding media. Compared to the metallic layer for plasmons, a dielectric multilayer for

#250804 Received 25 Sep 2015; revised 18 Nov 2015; accepted 19 Nov 2015; published 30 Nov 2015

BSWs shows several advantages, which make it a potential candidate for 2*D* optics. First, due to the use of dielectric material, the losses are very low. Therefore, the multilayer and the coupling configuration can be designed so that BSWs propagate over long distances. Another advantage is the possibility of operating within a broad range of wavelengths. Furthermore, because the maximum intensity associated with the BSW can be tuned on the surface, strong field intensity can be achieved on the interface and thereby enhance the light-matter interaction close to the surface. Additionally, the state of polarization of the BSWs may be chosen either to TE or TM, depending on the design of the multilayer.

In the past decade, BSWs have been reexamined and extensively utilized for mainly sensing applications. Several works have been proposed and demonstrated including experimental determination of BSWs sensitivity [5], direct comparison of BSWs and SPPs sensors [6], and the experimentally achieved improvement of sensitivity with BSWs in comparison with SPPs [7]. Among the sensing applications, we may cite those reported on chemical and biosensing [8–10], gas sensing [11], and fluorescence emission enhancement [12, 13]. Consideration of multilayer as a fundamental platform for 2*D* integrated optics providing sensing functionalities has started with some recent works. Among them, it has been shown by Descrovi et al. [14] that BSWs may be guided thanks to a dielectric waveguide on top of the multilayer. Furthermore, Sfez et al. [15] studied the refraction of surface waves at thin waveguide structures. The vision of the dielectric multilayer as a platform for two-dimensional integrated optics has been studied and demonstrated by studying a 2*D* lens [4] or simulating high-Q ring resonators [16].

In the following, we will use an exemplary BSW-sustaining multilayer as a suitable general platform for manipulating and control the BSWs propagation on its surface in the spectral range of telecom wavelengths. Several 2*D* optical photonic devices can be implemented starting from an ultra-thin ($\lambda/15$) polymer layer spun on the multilayer that can be subsequently shaped as desired. In particular, we study the BSW deflection effects caused by surface prisms. An experimental and theoretical study of the BSW diffraction through surface gratings is also performed.

2. Platform and experimental setup

The platform is designed to work in TE polarization at a center wavelength of 1.5 μm since experiments are carried out using an HP 81682*A* laser module. The corresponding wavelength ranges between $1.46\mu m$ and $1.58\mu m$. The multilayer consists of 12 layers of 263 $nm-$silicon oxide and 492 $nm-$silicon nitride, respectively. The refractive indices are 1.45 and 1.79 at 1.5 μm, respectively. On the top an 80 $nm-$thick layer of silicon nitride is deposited. The wide band-gad pf the multilayer (Bragg) allows a high tolerance in the fabrication process. Errors produced in fabrication can be easily compensated by adapting the coupe wavelength and incident angle. The thickness of the top layer defines the location of the dispersion line in the band gap, consequently, the properties of the propagation mode on the platform. Positive photoresist is then deposited on the platform. The presence of the polymer modifies the local effective refractive index, enabling direct manipulation of the BSW. The modification of the top surface to customize a 2*D* micro-system can be produced using e-beam writing, optical lithography or other patterning techniques. The propagation of surface waves through optical structures can be monitored by near-field imaging. A multi-heterodyne scanning near-field optical microscope (MH-SNOM) that allows amplitude, phase and polarization measurement is used in our experiments [15, 17].

The experimental setup is shown in Fig. 1(a) BSWs are excited using the Kretschmann configuration under the condition of total internal reflection (TIR). The sample (glass substrate with multilayer) is placed on a prism with index matching oil. The incident beam having an angle θ

#250804 Received 25 Sep 2015; revised 18 Nov 2015; accepted 19 Nov 2015; published 30 Nov 2015

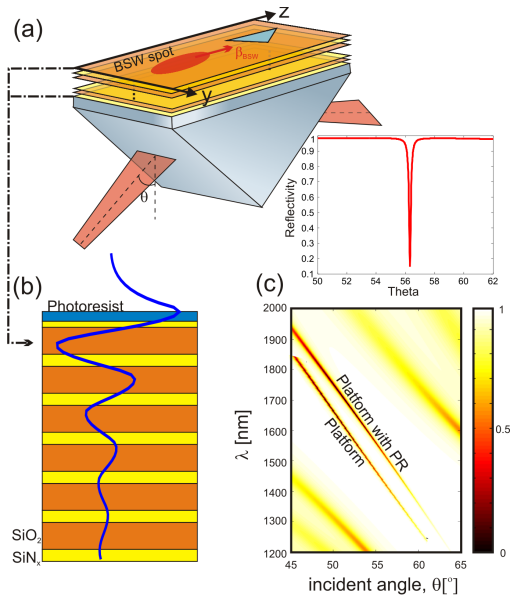

Fig. 1. (a) Schematic setup of the Kretschmann configuration for BSWs coupling along with the reflectance as a function of the incident angle. Optical polymer elements are engineered on top of the platform. (b) The platform consists of 6 periods of silicon nitride (263 nm, $n = 1.79$) and silicon dioxide (492 nm, $n = 1.45$) and of a top layer of silicon nitride (80 nm). (c) Calculated reflectance map of the multilayer as a function of the wavelength and the incident angle.

with the normal of the platform should match the following condition: $\beta = k \sin\theta$ in order to allow the excitation and the propagation of the BSW in the y-z plane. $k = n_g.2\pi/\lambda$ is the wave vector of the incident beam, β is the wave vector of the BSW, and θ is the incident angle. The different parameters of the platform are chosen so that the structure sustains BSWs and thus the mode can be confined at the top layer as shown in Fig. 1(b). The reflectance map, calculated using the transfer matrix method, is plotted as a function of the wavelength and the incident angle as shown in Fig. 1(c). The BSWs appears as a deep-dip below the light line. By adding a polymer layer on the top, the local effective index is modified as a function of its thickness, leading to a shift of the BSW. Thus, an effective index contrast (Δn) is created between the photoresist and the platform. The refractive index contrast is defined as the difference between the effective index of the BSW mode on bare platform ($n_{Platform}$) and the effective index of BSW mode for PR-coated platform (n_{PR}). This Δn is a key parameter for integrated optics, it is defined by the photoresist thickness and is limited by the band gap width. It is deduced from the dispersion relation: $n_{BSW} = \beta c/\omega$. In this work, prism and gratings are fabricated by a 100−thin layer of $AZ1518$ photoresist. The refractive index contrast is of $\Delta n = 0.05$.

In order to experimentally deduce the decay length,L, the field amplitude is measured as a function of the distance. By fitting this curve by an exponential law, we experimentally obtained a decay length of 628 μm [4], 7 times greater than the value recently obtained for the long-range SPPs studied by Lin et al. [23]. This corresponds to a propagation loss of $60 dB/cm$. Note that this value is far from the lower loss limit of the system. This decay is caused by the absorption of the material, surface scattering and the leakage into the prism. Since silicon nitride is low absorbent in the near infra-red and the fabrication show low roughness of the multilayer surfaces, the surface mode is weakly scattered by the film roughness. Thus the BSW amplitude is essen-

#250804 Received 25 Sep 2015; revised 18 Nov 2015; accepted 19 Nov 2015; published 30 Nov 2015

tially attenuated by the leakage into the prism. Nevertheless, leakage loss reduction should be possible by increasing the multilayer period number or adapting the coupling configuration

3. Two-dimensional polymer prism

In this section, we study a $2D$ prism working in total internal reflection (TIR). The device is schematically illustrated in Fig. 2(a). The incident beam is injected from the glass side of the platform. For a chosen incident angle of $\theta = 52.2^\circ$, which is higher than the critical angle for PR-coated platform ($n_c = 40.8^\circ$), the wavelength that allows the excitation of BSWs corresponds to 1542.2 *nm*. The incident beam is injected through through the prism. The projection of the focused spot on the platform has a diffraction-limited spot diameter of 30 μm in the coupling zone and propagates in the z direction. The incident beam is directed onto a $2D$ right angled polymer prism deposited on the multilayer platform. The prism is defined by its hypotenuse Λ. An example of prism topography ($\Lambda = 141.42\ \mu m$) is given in Fig. 2(b). The refractive index of the multilayer materials remain the same as those measured in the previous section of this paper because we are using the same platform. To work in TIR, the incident angle must be greater than 72.83°. As shown in Fig. 2(a), ξ is defined as the angle between the prism hypotenuse and the $y-$axis; η is the angle between the transmitted beam and the prism hypotenuse. We take an angle ξ of 74.8° and the wavelength of the incident beam is fixed to 1542.2 *nm*. The TIR effect is clearly seen in the measured near-field intensity distribution displayed in Fig. 2(c). An interference phenomenon appears at the top and the vicinity of the prism while almost no transmission of the electric field is seen at the left side of the prism.

The pattern is due to the interference between the transmitted beam T and the total internal reflected beam R as shown in the schematic of Fig. 2(a). In Fig. 2(d), we show the measured phase distributions in a $10\ \mu m \times 10\ \mu m$ area, which corresponds to the white square in Fig. 2(c). The interference patterns are remarkable and the shifts seen in the phase distribution confirms the interference behavior. By plotting in Fig. 2(e) an unwrapped phase along the z direction at a defined y (blue line in Fig. 2(d)), we can deduce the angle η and thus ξ from the slope $\tan\phi$ of the unwrapped phase curve:

$$\tan\phi = \frac{2\pi n_{PR}}{\lambda}\cos\eta \tag{1}$$

With Eq. (1), we obtain an angle η of $17^\circ\ 3^\circ$ and therefore ξ of $74.43^\circ\ 3^\circ$, which is close to value given in Fig. 2(a). The direction of the wave front is parallel to the hypotenuse verifying the interference between the transmitted and TIR signals.

4. Two-dimensional polymer gratings

This section discusses the diffracted field that arises through $2D$ gratings when an incident electromagnetic surface beam strikes the edge of a right-angle bend at an oblique angle γ. The incident beam illuminates the right angled isosceles gratings made in the PR layer. θ is adjusted by tilting the position of the gratings. The output beam lies in the platform plane and forms an angle α with respect to the normal of the gratings. We would like to notice that unlike previous experiments, in this section, the incident beam is directly coupled onto the PR layer. Its spot diameter is kept to 30 μm in order to include sufficient grating periods under illumination. Recall that the BSW can be generated for different couples (β, ω), therefore one can increase the incident angle θ and shift the wavelength to 1562.4 *nm*. In this case, the coupling condition falls onto the dispersion relation, where the coated 100 *nm* PR layer is considered (as seen in Fig. 3(a)). The proposed device is schematically illustrated in Fig. 3(a). Experimentally, we consider two gratings: one having a period Λ of 4 μm and a depth t of 2 μm, the other has a period of 6 μm and is 3 μm deep ($t = 3\ \mu m$).

#250804 Received 25 Sep 2015; revised 18 Nov 2015; accepted 19 Nov 2015; published 30 Nov 2015

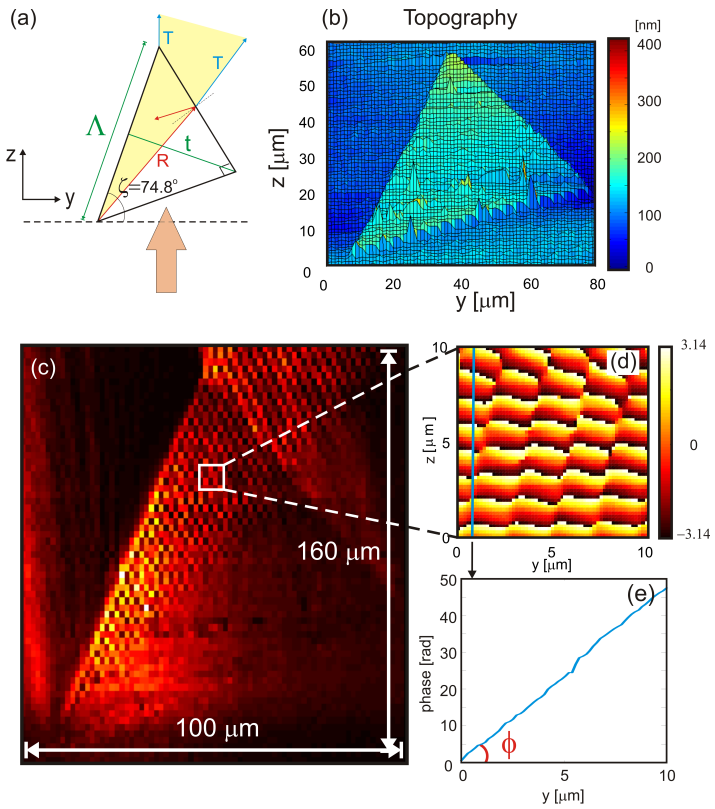

Fig. 2. (a) Schematic of a $2D$ right angled prism, Λ is the hypotenuse, ξ is the angle between the prism hypotenuse and the $y-$axis; η is the angle between the transmitted beam and the prism hypotenuse. (b) Topography of a 100 nm thin prism. (c) Measured near-field intensity at and nearby the prism. (d) Phase distribution of the inset area marked by a solid square in (c). (e) Plot of an unwrapped phase along z for a given y position.

Theoretically, the angles of the different diffraction orders can be calculated from the grating equation:

$$n_{platform}\sin\alpha_m = n_{PR}\sin\gamma + m\frac{\lambda}{\Lambda}, m = 0, \pm1, \pm2, \ldots \tag{2}$$

Where γ is the angle between the in-plane incident beam and the normal of the grating, α_m is the diffraction angle of the m^{th} order, λ is the incident wavelength, Λ is the grating period and m is an integer number that defines the diffraction order. Figure 3(b) shows the experimental near-field distribution for the 4 μm period grating illuminated by an incident angle $\gamma = 45^{circ}$. One can see a multi-wave interference pattern between the diffraction orders for each period of the grating. It should be noticed that even if we have two diffraction orders, only one propagation direction is seen on the platform area outside the gratings due to the interference. The bright area of the intensity distribution indicates the position of the 0^{th} order. The intensity of the other order (minus first order, $m = -1$) is weak, only interference between the two orders ($m = 0, -1$) is detected. Note that the scanning time of the intensity map taken over $100\mu m \times 100\mu m$ with a $1\mu m$ step is $100min$. In order to quantify the direction of the diffraction orders, a fine scan with a step of $\lambda/10$ is done in the marked 12 $\mu m \times 12$ μm square area and displayed in the inset of Fig. 3(b). Theoretical results obtained according to Eq. (2) and experimental results

#250804 Received 25 Sep 2015; revised 18 Nov 2015; accepted 19 Nov 2015; published 30 Nov 2015

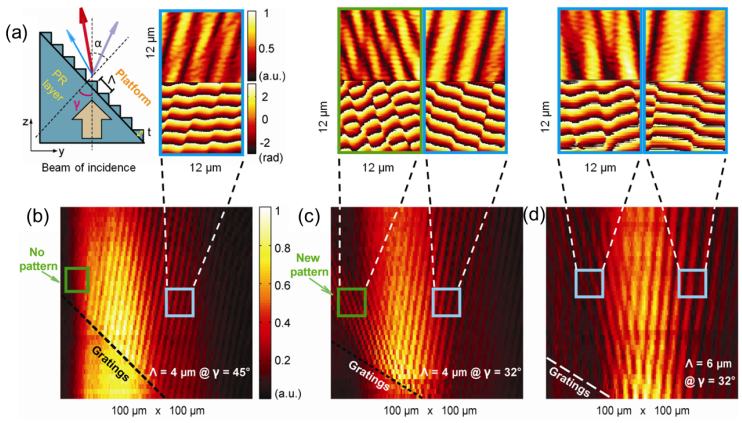

Fig. 3. (a) Schematic of a 2*D* gratings on top of a right angled prism, Λ is the grating period, γ is the incident angle, and α is the angle between the normal and n^{th} diffracted order. (b) and (c) show the intensity distribution of a $4\mu m$ period grating. The incident angle is 45° and 32°, respectively. (d) Intensity distribution of a $6\mu m$ grating illuminated with an incident angle of 32°. The insets of figures (b), (c), and (d) show the phase distribution along with the intensity distribution of the areas defines by squares.

are compared in Table 1. It shows the angles for the different diffraction orders as well as the interference between them. Using the same method described in the previous section (Fig. 3(e)), the interference pattern has an angle $\alpha = 36^\circ \pm 3^\circ$ which is in a good agreement with the calculated interference angle 35.99° between the 0^{th} and the -1^{st} orders. In Fig. 3(c), the incident angle γ is decreased to 32°, one more diffraction order appears at the left side of the 0^{th} order, and it only owns a part of the whole field energy. There are two interference patterns, one between the 0^{th} and the 1^{st} diffraction orders and a second between the 0^{th} and the -1 orders. The measured angles, obtained from the inset phase of Fig. 3(c), are $\alpha = 48^\circ \pm 3^\circ$ and $\alpha = 23^\circ \pm 3^\circ$, respectively which are close to the calculated values shown in Table 1. The new interference pattern is indicated by a green solid square in Fig. 3(c) compared to the dark area in Fig. 3(b) where the 1^{st} diffraction order does not exist. In Fig. 3d, we kept the incident angle to 32° but the used grating period is 6 μm in order to confirm the effect of the grating period value on the interfered light. There are diffraction orders (1, 0 and -1) and two interference regions having $42^\circ 3^\circ$ and $26.4^\circ 3^\circ$ respectively. In addition, one can clearly observe that the fringe spacing is proportional to the period. One can see a very good agreement between theory and the near-field measurement.

As can be seen from Fig. 3(b)–3(d), most field intensity is concentrated in the 0^{th} order. This is due to the weak refractive index contrast Δn (0.055) of the device. In order to obtain better efficiency, the optical path difference should satisfy $\Delta nt = \lambda$. Therefore, taken the current refractive index contrast ($\Delta n = 0.055$), increasing the efficiency can be obtained by increasing the structure thickness up to $t = 28.4\ \mu m$, which is about 18 times the wavelength. Other possibility is to decrease the wavelength in order to have smaller thickness but t will remains greater than λ. This could be a challenge in spacing downscale of the structure size in integrated optics. However, one can increase the refractive index contrast Δn to $\lambda/t = 0.78$ keeping the grating thickness to 2 *m* for full diffractive efficiency. Consequently, we confirm that the effective index contrast Δn is a critical parameter that provides an efficiency improvement for minia-

#250804 Received 25 Sep 2015; revised 18 Nov 2015; accepted 19 Nov 2015; published 30 Nov 2015

Table 1. Theoretical and measured angles of the interference pattern.

A Angle of diffraction orders (theory)
B Angle of the interference pattern between the corresponding diffraction orders (theory)
C Angle of the interference pattern (experiments, ±3°)

Gratings		1^{st} order (α_1)	0^{th} order (α_0)	-1^{st} order (α_{-1})
Λ = 4 μm @ γ = 45°	A	-----	47.74°	24.25°
	B	-----	35.99°	
	C	-----	36°	
Λ = 4 μm @ γ = 32°	A	62.12°	33.68°	13.02°
	B	47.90°	23.35°	
	C	48°	23°	
Λ = 6 μm @ γ = 32°	A	50.73°	33.68°	19.58°
	B	42.21°	26.63°	
	C	42°	26.4°	

turized structures. The 2*D* grating element may be an interesting solution for the investigation of Dammann gratings on the BSW based platform. By an appropriate design of the diffractive grating working in transmission, the diffracted wave can be modulated so that it generates a fun-out function.

5. Conclusion

In conclusion, 2*D* polymer optical elements are fabricated on top of the BSWs sustaining multilayer. Due to the low loss property of the dielectric-based multilayer, the platforms provides 628 μm of propagation length which is approximately 7 times what is obtained for SPPs. These properties offer a powerful platform with low propagation loss and high-energy source for 2*D* optics. Reflections and diffractions of BSWs are experimentally studied with 10 $nm-$thickness of polymer prism and two gratings with the aid of a multi-heterodyne scanning near-field optical microscope (MH-SNOM). Total internal reflection is verified by studying the near-field amplitude-phase of the reflected field on the hypotenuse. Next, the diffracted field that arises through 2*D* gratings when an incident electromagnetic surface beam strikes the edge of a right-angle bend at an oblique angle is observed in the near-field and analyzed. The measured angle of interference pattern which is caused by the diffraction orders agree with the theoretical prediction.

Acknowledgments

This work is supported by the Swiss National Science Foundation (SNSF). The authors would like to thank Dr. Emiliano Descrovi for his knowledge and his support in understanding the multilayer and its property characterization work. The authors would like to thank Dr. Toralf Scharf and Mme. Irène Philipoussis Fernandez for the photoresist deposition.

#250804 Received 25 Sep 2015; revised 18 Nov 2015; accepted 19 Nov 2015; published 30 Nov 2015